Quasi-planar InGaAsSb *p*-B-*n* photodiodes for spectroscopic sensing

L. A. Hanks[1,*], K. Mamic[1], K. Kłos[2], A. Bainbridge[1], J. Fletcher[1], L. Gilder[1], L. Tedstone[1], F. J. Castaño[3] and A. R. J. Marshall[1]

[1]*Department of Physics, Lancaster University, Lancaster LA1 4YB, United Kingdom*
[2]*Photin LLC, 05-080 Klaudyn, Poland*
[3]*ams OSRAM AG, Technology R&D, Tobelbader Strasse 30, 8141 Premstaetten, Austria*
**l.hanks@lancaster.ac.uk*

Abstract: An InGaAsSb *p*-B-*n* structure has been designed and characterised for zero bias low power detection applications. Devices were grown by molecular beam epitaxy and fabricated into quasi-planar photodiodes with a 2.25 µm cut-off wavelength. Maximum responsivity was measured to be 1.05 A/W at 2.0 µm, achieved at zero bias. $D*$ of 9.4×10^{10} Jones was determined from room temperature spectra of noise power measurements with calculated $D*$ remaining >1×10^{10} Jones up to 380 K. With a view to simple miniaturised detection and measurement of low concentration biomarkers, optical powers down to 40 pW were detected, without temperature stabilisation or phase-sensitive detection, indicating the photodiode's potential.

1. Introduction

Beyond the cut-off wavelength of $In_{0.53}Ga_{0.47}As$ and GaSb at ~1.7 µm, a host of environmentally and socially impactful substances exhibit absorption peaks, including glucose, acetone and carbon dioxide, relevant to diabetes management, cancer detection and environmental monitoring respectively. Useful sensing applications of such substances require accurate detection of small concentrations and hence high sensitivity photodetectors. Of particular interest is the expansion of commercial electronics applications such as wearable blood glucose monitors where in a healthy person glucose typically ranges from 4 mmol/L to 7 mmol/L and is as high as 20 mmol/L in diabetics [1]. In order to evaluate capability for such applications, detectors need to be assessed within the regime of low optical power resolution and hence low noise.

GaSb substrates can accommodate lattice matched epilayers exhibiting cut-off wavelengths from the near to the longwave infrared. For detectors in the mid and longwave infrared GaSb is rapidly becoming the dominant substrate, however currently to detect wavelengths between 1.7 µm and 2.6 µm, lattice-mismatched InGaAs photodiodes grown on InP are commonly used. Relaxation associated with the metamorphic growth produces defects, reducing the potential performance. InGaAsSb allows for a composition-tuned cut-off wavelength up to approximately 2.6 µm, whilst avoiding the Ga rich limit of the miscibility gap and maintaining lattice matching to GaSb, to avoid relaxation related defects. Hence, there is potential for InGaAsSb to facilitate GaSb becoming a one-stop substrate of choice for IR detectors operating beyond silicon's cut-off wavelength. Moreover, GaSb can easily be grown on GaAs substrates via an interfacial misfit array layer, and substantial progress has been made on buffers to growing GaSb directly onto silicon substrates, expanding commercial options [2,3]. InGaAsSb shortwave infrared detectors are currently being reported with both *p*-*i*-*n* and *n*B*n* device structures [4,5].

This work presents a *p*-B-*n* $In_{0.14}Ga_{0.86}As_{0.1}Sb_{0.9}$ photodiode with a quasi-planar structure and cut-off wavelength of 2.25 µm. The built-in field from the *p*-*n* junction allows room temperature operation at 0 V, while the barrier and quasi-planar structure helps to reduce leakage. Together these characteristics make the *p*-B-*n* architecture desirable for certain industry applications. Even accounting for the small valence band offset (VBO) calculated to be ~20 meV it operates at 0 V. More Shockley–Read–Hall processes and thus leakage is expected than in a traditional *n*B*n*. Work from Nong Li et al. has shown that under a small applied bias of -50 mV, non-planar *p*-B-*n* photodiodes in this material have improved leakage over *n*B*n* photodiodes despite an inbuilt field [6]. Planar photovoltaic devices typically require diffusion or implantation whereas this work uses only a simple shallow etch and appropriate epitaxial doping concentrations. The quasi-planar nature eases fabrication, produces reliable devices without an exposed junction and produces a near-level surface to further fabricate on. The photodiodes in this work show comparable D^* to commercially available extended InGaAs detectors, despite being in their infancy in terms of material optimisation.

2. Growth and sample design

The structure shown in the inset of Fig. 1 (a) was grown by molecular beam epitaxy on an *n*-GaSb substrate, designed in a front illuminated configuration. Photodiodes of circular shape and 280 µm diameter were fabricated using standard photolithography and wet-etching techniques with Ti/Au metallisation. The optical window is formed of an area of 46500 μm^2 excluding the top contact area. The shallow device mesa was defined just to the barrier and the common contact was deposited at a depth of ~400 nm into the absorber. An additional photodiode array was fabricated with Si_3N_4 deposited as a passivation and anti-reflection layer which covered the whole surface with exception to the contact area. Leakage current measurements were performed in the dark using a Lakeshore TTPX probe station, with Keithley 2400 and 6430 source meters. An Agilent E4980A LCR meter was used to carry out capacitance-voltage measurements. Spectral response was conducted using both a Bruker V70 FTIR spectrometer and a Bentham PVE300 monochromator system with a flood-illuminated measurement set up. Noise power spectra were measured using an Agilent 35670A dynamic signal analyser.

The epi-structure growth commenced with a GaSb buffer and an $In_{0.14}Ga_{0.86}As_{0.1}Sb_{0.9}$ *n*-cladding layer, lattice matched to GaSb, followed by a 2.0 µm thick *n*-$In_{0.14}Ga_{0.86}As_{0.1}Sb_{0.9}$ absorber layer with tellurium used as the *n*-type dopant. A low doped *p*-$Al_{0.2}Ga_{0.8}Sb$ layer provides the 60 nm barrier, finally a 200 nm *p*-GaSb layer aids ohmic contacting and caps the structure with optical transparency, with beryllium used as the *p*-type dopant. The dopant was chosen by the electric field simulations in Fig.1 (b). The non-lattice matched barrier layer is within the critical thickness defined by the Matthews and Blakeslee model [7].

The band structure, shown in Fig. 1 (a), was simulated using nextnano with band parameters from Vurgaftman et al. [8,9]. The aluminium percentage was selected to achieve a minimal offset in the valence band between InGaAsSb and AlGaSb, calculated to be 20 meV, promoting hole conduction, with the conduction band offset of 180 meV between the GaSb and AlGaSb layers reducing electron conduction. Capacitance-voltage measurements were carried out and the depletion width found through simulation. The simulation parameters included thicknesses and dopant concentrations verified by SIMS measurements, permittivity's were taken from the literature where available or calculated using Vegard's law [10]. In Fig. 1 (a) the shaded regions within the band structure indicate the depletion region around the type junction at zero bias, the *p*-type barrier is fully depleted, the *n*-type side is depleted up to 24 nm. Thus, this structure is heavily reliant on diffusion rather than drift, for collection of photogenerated holes from the absorber. The hole diffusion length in InGaAsSb was reported by Craig et al. to be ~11 µm at room temperature [11].

Optical transmission through the structure was calculated using an absorption coefficient of 6800 cm^{-1} at 2.1 µm for In$_{0.14}$Ga$_{0.86}$As$_{0.1}$Sb$_{0.9}$, based on characterisation of single In$_{0.14}$Ga$_{0.86}$As$_{0.1}$Sb$_{0.9}$ epilayers. For other materials literature values were used. The absorber absorbs ~ 77 % of light at a wavelength of 2.1 µm and ~85 % of light at a wavelength of 1.55 µm.

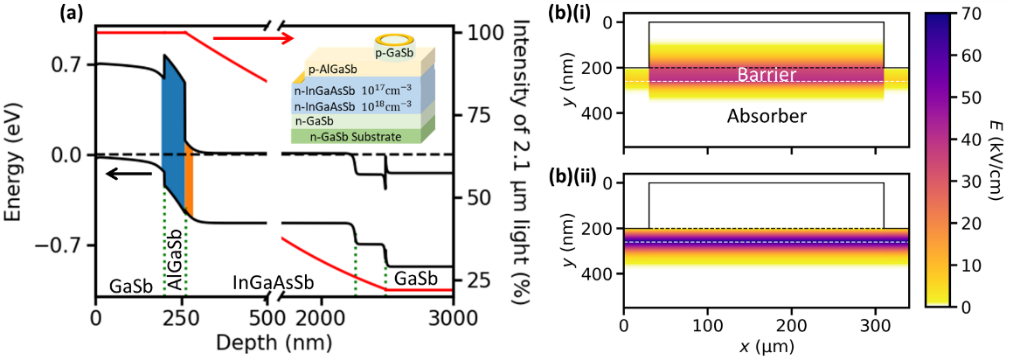

Fig. 1. (a) Band structure (black lines) modelled at 0 V is shown on the left axis, with the Fermi level (dashed). The growth direction is from right to left and layer interfaces are indicated (green dotted). Note the broken x-axis and change in scale either side. The calculated depletion width either side of the junction is shown by shading within the band structure. Absorption of 2.1 µm light through the structure (red line) is shown on the right axis. Inset shows the epilayer structure and the device physically separated from the lower contact. (b) Simulated electric field magnitude; x and y (growth direction) indicate spatial dimensions, dashed lines represent the boundary of the barrier, solid line represents the mesa outline. (i) Barrier doping concentration of 1× 10^{16} cm^{-3} showing no significant lateral field spreading. (ii) Barrier doping concentration of 1 × 10^{17} cm^{-3}, showing deleterious lateral field spreading.

A 2D electric field around the junction was simulated using nextnano through evaluation of Poisson's equation, the lateral spreading of the electric field within the barrier was sensitive to doping concentration, as shown in Fig. 1(b). In this work the barrier doping is sufficiently low to supress spreading and essentially confine the field to the mesa area and thus allow for a successful implementation of the quasi-planar architecture. Suppression of lateral carrier collection and hence crosstalk, was confirmed by a measurement of position dependent photocurrent, induced by a laser. The illumination spot was scanned from the mesa top to the barrier and accounting for the intensity distribution of the spot, the lateral carrier collection length was found to be 3 µm. If the barrier doping was increased, the field would spread beyond the mesa area, increasing the carrier collection volume and risking crosstalk. Such higher barrier doping would necessitate a deep mesa etch to isolate individual photodiodes.

3. Electrical characterisation

Leakage current density within a temperature range of 77 K - 360 K is shown in Fig. 2 (b); measured using an IR shielded probe station. Temperatures above room temperature were considered to reflect standard operating temperature ranges for consumer electronic devices. Below 240 K the leakage current at near zero bias voltages is influenced by the noise floor of the measurement set-up producing a non-photovoltaic measurement artefact, evident in the current minimum moving into the forward bias. This occurs as the current measurement becomes dominated by a negative input offset current within the source meter.

An Arrhenius plot of leakage current density against temperature is shown in Fig. 2 (a). At 240 K the zero bias current density is compromised by the measurement floor as shown by the moving minimum measurement artefact in Fig. 2 (b). Near 0 V the activation energy (E_a) was 0.351 eV, reducing to approximately half band gap for this material (Eg = 0.66 eV at 0 K) at a bias voltage of 100mV, indicating Shockley-Read-Hall is the dominant contributor to the leakage current [12]. All measurements were taken in an IR shielded probe station. Elevated activation energies at low bias voltage this have been reported in *n*B*n*'s where E_a is increased due to a valence band offset at the barrier, the effect reducing with increasing bias voltage [13]. The same effect is attributed to the small elevation in activation energy observed here. Perimeter/area dependence of leakage current indicated that the detectors were not bulk limited, as such the true potential of these photodiodes has not yet been reached. Work from Shafir et al. has shown that diffusion limited current is possible in InGaAsSb at room temperature with a homojunction *p*-*n* photodiode [14]. Thus, there is scope for improvement in the photodiodes reported here.

R_0A, was calculated to be 150 Ωcm^2 at room temperature, this is approximately a factor of 4 below the R_0A given by Rule 17 ~600 Ωcm^2 for InGaAs with a 2.3 µm cut-off [15]. Rule 17 is an empirical rule created by Zang et al. to approximate figures of merit for extended InGaAs at a range of temperatures and cut-off wavelengths. Within the work of Zang et al. saturation current is calculated from the resistance area product by $J_s = k_BT/qR_0A$. Using this equation J_s is calculated to be 1.75×10^{-4} Acm^{-2} at room temperature, whereas Zang et al. suggest ~1.0×10^{-4} Acm^{-2}, for extended InGaAs with a 2.3 µm cut-off wavelength.

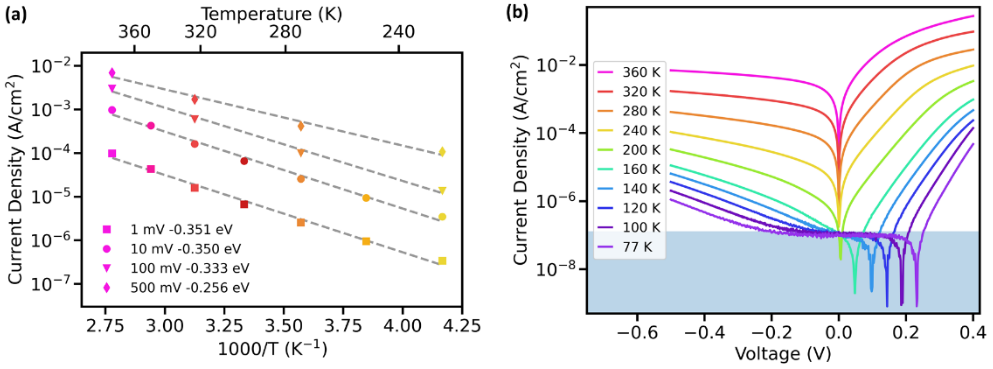

Fig. 2. (a) Magnitude of leakage current density Arrhenius plot at select reverse bias voltages, 1 mV (square), 10 mV (circle), 100 mV (inversed triangle) and 500 mV (diamond), activation energy is annotated for each bias. (b) Magnitude of leakage current as a function of bias for temperatures from 77 K- 360 K, with the measurement noise floor indicated by the shaded area.

4. Optical characterisation and noise evaluation

The spectral response of a photodiode, fabricated with a 280 nm Si_3N_4 passivation and antireflection coating, is shown in Fig. 3. The cut-off wavelength, taken to be 50% of the maximum response, is ~2.25 µm. The external quantum efficiency, EQE, for a wavelength of 2.0 µm is 63 %, corresponding to a peak responsivity of 1.05 A/W. This is comparable to commercially available extended InGaAs with a peak responsivity of 1.10 A/W and a cut-off wavelength of 2.3 µm [16]. Importantly, the $In_{0.14}Ga_{0.86}As_{0.1}Sb_{0.9}$ photodiode maintains a high quantum efficiency for all wavelengths between the cut-off wavelength of silicon (~1.0 µm) and its own cut-off wavelength [17].

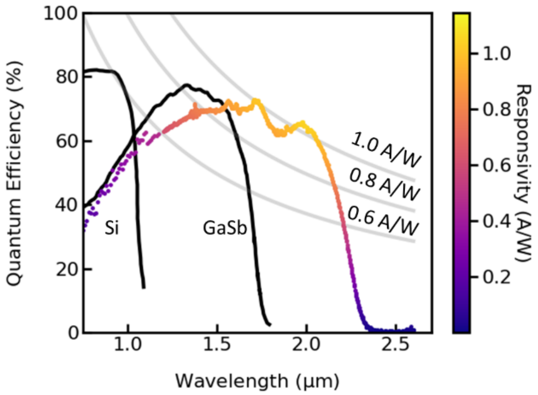

Fig. 3. Spectral quantum efficiency measured at room temperature and 0 V, for the InGaAsSb *p*-B-*n* detector with an anti-reflection coating (data with colour gradient). Incident optical power density was ~400 µW/cm^2 at 2µm. Responsivity contour lines are also shown in grey as a guide. Silicon and GaSb quantum efficiencies are shown for comparison (black lines) [17,18].

The specific detectivity, $D*$, was initially estimated by the common equation

$$D^*\,(\lambda) = \frac{\mathrm{QE}(\lambda)\,\frac{\lambda q}{hc}}{\sqrt{\frac{4k_B T}{RA} + 2qJ}}, \qquad (1)$$

where λ is the wavelength, R is the dynamic resistance, T is temperature, J is current density, A is device area and q, h, c, and k_B are physical constants [6]. Both shot and Johnson noise were assumed to contribute for this calculation. At 2.0 µm $D*$ reaches ~ 1×10^{11} Jones at 0 V, commercially available InGaAs with a cut-off of 2.2 µm has a $D*$ ~ 3×10^{11} Jones [16]. Bias dependence of $D*$ shows a maximum at 0 V. Johnson and shot noise contributions to the $D*$ were also considered independently, where Johnson noise current is $i_{nj} = \sqrt{4k_B T \Delta f / R}$ and shot noise current is $i_{ns} = \sqrt{2qI\Delta f}$, where Δf represents the bandwidth of the measurement. Close to the operating bias of 0 V, $i_{nj} = 2 \times 10^{-13}$ A / Hz$^{1/2}$ and $i_{ns} = 3 \times 10^{-15}$ A / Hz$^{1/2}$. Thus, Johnson noise is dominant at 0 V, which remains the case up to -40 mV in the reverse. To confirm the estimated $D*$ from calculation, the noise power spectrum was measured at 0 V and room temperature, between 10 Hz and 3 kHz. The measurement was verified through comparison to the Johnson noise measured on resistors.

Comparison to previously reported InGaAsSb photodiodes with a low In fraction, operating at zero bias, is given in Table 1. This work shows increased R_0A which is attributed to the barrier reducing leakage current. Though Nunna et al. did not have a barrier their structure included an interfacial misfit array layer within the current path, between the GaAs substrate and the GaSb buffer, which increased series resistance. The peak responsivity in this work is high with respect to others with longer cut-off wavelengths. Together, this leads to a $D*$ which is greater than previously reported in this material.

Fig. 4 (a) shows the close agreement between calculated Johnson noise and measured spectral power density for a selection of resistors and the *p*-B-*n* photodiode. The noise was flat across the bandwidth measured with the exception of a background noise comb, originating from the 50 Hz line supply. The noise floor of the meter was characterised to be 2×10^{-8} V/$\sqrt{\mathrm{Hz}}$, the equivalent of Johnson noise on a 40 kΩ resistor. The resistance of the $In_{0.14}Ga_{0.86}As_{0.1}Sb_{0.9}$ photodiode was determined from leakage current measurements to be 240 kΩ and its noise was measured to be in line with theoretical calculations for Johnson noise given this resistance. This ideal Johnson noise behaviour is further confirmed by the almost identical noise spectrum measured for comparison on a 270 kΩ resistor. Furthermore, within the frequency range characterised, no appreciable $1/f$ noise is observed.

Table 1. Figures of Merit for Photovoltaic InGaAsSb Photodiodes with Differing Indium Concentrations

	In 14% This work	In 15% Salesse et al.	In 18% Nunna et al.	In 20% Prineas et al.	In 24% Shao et al.
Ref		[19]	[20]	[21]	[22]
R_0A at 300 K (Ωcm^2)	150	15	260	25	90
Peak responsivity (A/W)	1.05	0.35	0.8	1.0	1.16
Cut-off wavelength (µm)	2.25	2.2	2.4	2.4	2.6
D^* ($\times 10^{10}$ Jones) at 0 V	9.7	~1	4.5	6	0.9

The D^* calculated using the measured power spectrum and the more common best-case estimate approach using Eq. (1), are both shown in Fig. 4 (b). The agreement between them confirms that in these photodiodes the noise is indeed Johnson dominated at 0 V, without any significant increase due to nonidealities unaccounted for by the best-case approach. Such agreement is not always obtained when true noise powers are measured. D^* was calculated against wavelength between 252 K and 377 K using Eq. (1) and leakage current data. Below 250 K the current is influenced by the noise floor, imposing a lower limit. As the temperature decreases, D^* moves towards the background limited performance of photovoltaic detectors [23]. The increase in D^* with decreasing temperature is comparable to that reported for extended InGaAs with a 2.6 µm cut-off [16]. Since E_a has been measured as half band gap, indicating non-ideal Shockley-Read-Hall is a dominant contributor to leakage current, improvement in material quality could result in closer to diffusion limited leakage and hence an enhancement in D*.

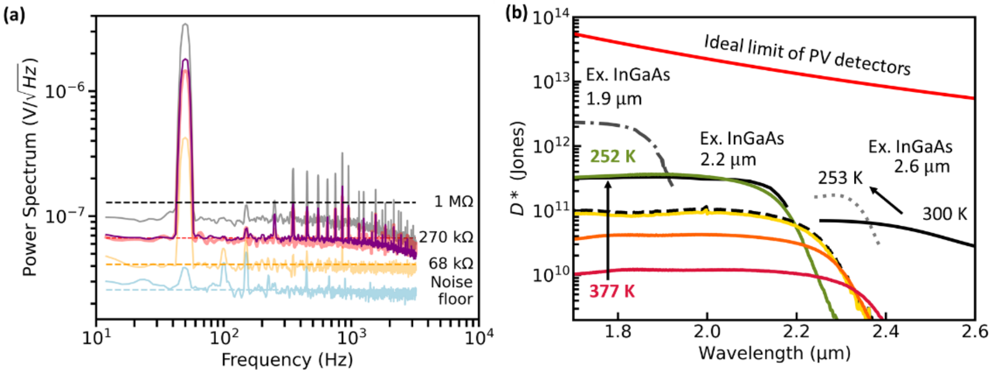

Fig. 4. (a) Noise power spectra measured at room temperature for resistors of 68 kΩ (orange), 270 kΩ (red), 1 MΩ (grey) and the InGaAsSb photodiode which has a dynamic resistance of 240 kΩ at 0 V (purple). Calculated Johnson noise for each resistor value (dashed) is included for comparison. (b) Calculated specific detectivity against wavelength for a series of temperatures at 0 V, 377 K (pink), 335 K (orange), 301 K (yellow) and 252 K (green). D^* from measured noise at room temperature is shown as a dashed line. D^* for commercially available InGaAs with three cut-off wavelengths is shown in solid black at room temperature with the 2.6 µm cut-off also shown at 253 K (dotted) [16, 23]. Background limited spectral detectivity is shown in red [23].

The magnitude of absorption exhibited by low concentration biomarkers, can be small within relevant medical concentration ranges. The measurement challenge is further exacerbated by high total absorption when sensing compounds in solution. Thus, small changes in relatively low total optical powers need to be precisely resolvable. Low optical powers were measured with the InGaAsSb photodiode to demonstrate and determine the resolution limit of the photodiode in this work. A 1 mW, 1.55 µm laser source was used in an underfilled fibre coupled arrangement and was incrementally attenuated to a minimum power of 3.3 pW. A small-area fibre-coupled $In_{0.53}Ga_{0.47}As$ photodiode and a fibre splitter provided a simultaneous real-time reference measurement of the laser's optical power provided to the device. As shown in Fig. 5 the photocurrent was linearly dependent on optical power from ~100 pW to 50 µW, thus the responsivity is constant in this range and noise evidently low. Optical powers are resolvable to 10's pW based on a simple constant leakage current subtraction, below this the measurement was unstable due to noise sources within the probed and thermally unregulated measurement set-up, which in practice exceeded the photodiode's Johnson noise limit. The calculated Johnson noise limit for a S/N ratio of 1, based on the estimated measurement bandwidth, is only reached at ~2 pW of optical power. Hence improvements in low power resolution are expected when a detector is integrated with dedicated measurement circuity. Under high optical power, the photocurrent saturates due to high series resistance in the *n*-type contacts. With high GaSb concentration, the InGaAsSb contacting layer exhibits a GaSb nature, and associated challenges in creating a low resistance *n*-type ohmic contact [24]. Obtaining low contact resistance was not a focus of this work hence it is reasonable to expect reductions in contact resistance with refinement of the processing.

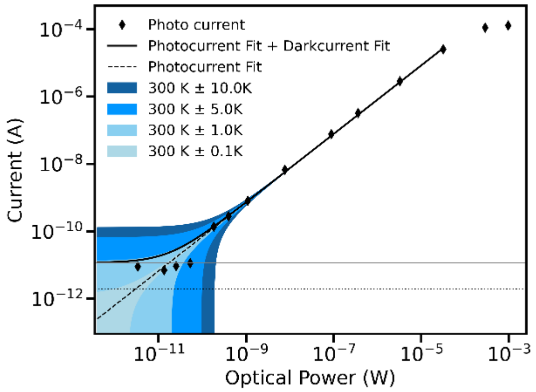

Fig. 5. Current against optical power at room temperature. Measured photocurrent (diamonds), linear fit of photocurrent (dashed black), total current (black line), leakage current (grey line), estimated Johnson noise current (dotted). Shades of blue indicate error band in the inferred photocurrent due to temperature changes from 300 K within ΔT of 0.1 K, 1.0 K, 5.0 K and 10 K, using a temperature invariant leakage current subtraction.

Small photocurrents are often measured using phase sensitive techniques, to account for any changes in leakage current. However, in low-cost consumer electronics this is not always feasible and calculation of photocurrent based on subtraction of a fixed leakage current is desirable. Using the characterised dependence of leakage current on temperature, the inferred photocurrent based on a fixed, assumed temperature invariant, leakage current subtraction was calculated for different fluctuating actual temperature ranges. It is shown in Fig. 5 that for optical powers greater than ~1 nW, temperature fluctuations up to ± 10 K will have negligible effect on the inferred photocurrent, thus subtraction of a fixed leakage current can be sufficient. However, below 0.01 nW optical power, the inferred photocurrent becomes significantly erroneous for even a 1 K temperature change. Therefore, the concentration of the substance being detected would be miscalculated. In this regime, precise temperature correction or phase sensitive detection, would be essential. To further relate the low optical power measurements to the intended application the magnitude of change in optical power expected due to changes in glucose concentrations was calculated. Considering an input optical power of 1 mW and a nominal optical pathlength of 1 mm, the absorbance for a glucose solution was evaluated through Beer-Lamberts law using absorptivity's given by Amerov et al. [25]. As water exhibits significant absorption in the near-infrared, water displacement by glucose must be considered, the water displacement factor is also given in Amerov et al. [25]. Within the 4 – 7 mmol/L healthy range, the optical power change for a 0.1 mmol/L difference is calculated to be 3.4×10^{-9} W, which is within the linear region shown in Fig. 5 and hence resolvable. Indeed, this also exceeds the potential uncertainty band originating from fluctuations in the photodiode temperature.

5. Conclusion

This work has demonstrated quasi-planar InGaAsSb photodiodes with a 2.25 μm cut-off wavelength, achieving a high D^* of 9.4×10^{10} Jones with zero-bias room temperature operation, using simple processing techniques. Maximum responsivity is measured to be 1.05 A/W at 2.0 μm approaching values of commercial extended InGaAs and higher than previous low indium fraction InGaAsSb photodiodes. Optical powers down to 40 pW were detected and resolved with a simple probed measurement set-up. Excellent Johnson limited noise characteristics were measured, without evidence of $1/f$ noise, highlighting the potential for this detector to enable the measurement of low concentration biomarkers, once integrated with optimised circuitry.

Funding. This work was supported by EPSRC Impact Acceleration Account for funding under Grant No. EP/R511560/1.

Disclosures. The authors declare no conflicts of interest.

Data availability. Data underlying the results presented in this paper are available in Lancaster University Research Portal, reference number 364413409.

References

1. D. Levy, *The Hands-On Guide to Diabetes Care in Hospital* (John Wiley & Sons, Incorporated, Newark, 2015) p.11.
2. S. H. Huang, G. Balakrishnan, and D. L. Huffaker, "Interfacial misfit array formation for GaSb growth on GaAs," J. Appl. Phys. **105**, 103104-1-5 (2009).
3. E. Delli, V. Letka, P. D. Hodgson, E. Repiso Menendez, J. Hayton, A. P. Craig, Q. Lu, R. Beanland, A. Krier, A. R. J Marshall, and P. J. Carrington, "Mid-Infrared InAs/InAsSb Superlattice nBn Photodetector Monolithically Integrated onto Silicon," ACS Photonics **6**, 538-544 (2019).
4. N. Li, G. Wang, D. Jiang, W. Zhou, F. Chang, F. Lin, W. Chen, J. Jiang, X. Xu, L. She, S. Cui, B. Liu, H. Hao, D. Wu, Y. Xu and Z. Niu, "Trap-assisted tunneling current and quantum efficiency loss in InGaAsSb short wavelength infrared photo detectors," Semicond. Sci. Technol. **37**,115010 (2022).
5. N. Li, J. Sun, Q. Jia, Y. Song, D. Jiang, G. Wang, Y. Xu and Z. Niu, "High performance nBn detectors based on InGaAsSb bulk materials for short wavelength infrared detection," AIP Adv. **9**, 105106 (2019).
6. N. Li, W. Chena, D. Zheng, J. Sun, Q. Jia, J. Jiang, G. Wang, D. Jiang, Y. Xua, and Z. Niu, "The investigations to eliminate the bias dependency of quantum efficiency of InGaAsSb nBn photodetectors for extended short wavelength infrared detection," Infrared Phys. Technol. **111**, 103461 (2020).
7. J. W. Matthews and, A. E. Blakeslee, "Defects in epitaxial multilayers: I. Misfit dislocations," J. Cryst. Growth **27**, 118-125 (1974).
8. S. Birner, S. Hackenbuchner, M. Sabathil, G. Zandler, J.A. Majewski, T. Andlauer, T. Zibold, R. Morschil, A. Trellaskis, and P.Vogl, "Modeling of Semiconductor Nanostructures with nextnano^3," Acta. Phys. Polonica. A **110**, 111-124, (2006).
9. I. Vurgaftman, J. R. Meyer, and L. R. Ram-Mohan, "Band parameters for III–V compound semiconductors and their alloys," J. Appl. Phys. **89**, 5815-5875 (2001).
10. S. Zollner, C. Lin, E. Schönherr, A. Bohringer, and M. Cardona, "The dielectric function of AlSb from 1.4 to 5.8 eV determined by spectroscopic ellipsometry," J. Appl. Phys. **66**, 383-387 (1989).
11. A. P. Craig, M. Jain, G. Wicks, T. Golding, K. Hossain, K. McEwan, C. Howle, B. Percy, and A. R. J. Marshall, "Short-wave infrared barriode detectors using InGaAsSb absorption material lattice matched to GaSb," Appl. Phys. Lett. **106**, 201103-1-4 (2015).

12. A. P. Craig, M. D. Thompson, Z-B Tian, S Krishna, A. Krier, and A. R. J. Marshall, “InAsSb-based nBn photodetectors: lattice mismatched growth on GaAs and low frequency noise performance,” Semicond. Sci. Technol. **30**, 105011-1-7 (2015).
13. J. Pedrazzani, “Characteristics of InAs-Based nBn Photodetectors Grown by Molecular Beam Epitaxy,” Doctoral Dissertation, University of Rochester (2010).
14. I. Shafir, N. Snapi, D. Cohen-Elias, A. Glozman, O. Klin, E. Weiss, O. Westreich, N. Sicron, and M. Katz, “High responsivity InGaAsSb p–n photodetector for extended SWIR detection,” Appl. Phys. Lett. **118**, 063503-1-4 (2021).
15. Y. Zhang, Y. Gu, X. Chen, Y. Ma, X. Li, X. Shao, H. Gong, and J. Fang, “IGA-rule 17 for performance estimation of wavelength-extended InGaAs photodetectors: validity and limitations,” Appl. Opt. **57**, D141-D144 (2018).
16. Teledyne Judson Technologies, “J22 and J23 SERIES InGaAs PHOTODIODES Operating Instructions,” http://www.teledynejudson.com/prods/Documents/PB4206.pdf.
17. M. Vollmer, K. Möllmann, and J. A. Shaw, “The optics and physics of near infrared imaging” in ETOP 2015 Proceedings, Bordeaux, France, 29 June–2 July (2015), edited by E. Cormier, L. Sarger pp 97930Z-1-8.
18. J. Tournet, “III-Sb-based solar cells and their integration on Si,” Doctoral Dissertation, Université De Montpellier (2019).
19. A. Salesse, A. Joullié, P. Calas, J. Nieto, F. Chevrier, Y. Cuminal, G. Ferblantier1, and P. Christol, “Surface passivation of GaInAsSb photodiodes with thioacetamide,” Phys. Stat. Sol. (c) **4**, 1508 (2007).
20. K. C. Nunna, S. L. Tan, C. J. Reyner, A. R. J. Marshall, B. Liang, A. Jallipalli, J. P. R. David, and D. L. Huffaker, “Short-Wave Infrared GaInAsSb Photodiodes Grown on GaAs Substrate by Interfacial Misfit Array Technique,” IEEE Photon. Technol. Lett. **24**, 218-220 (2012).
21. J. P. Prineas, J. Yager, S. Seyedmohamadi, and J. T. Olesberg, “Leakage mechanisms and potential performance of molecular-beam epitaxially grown GaInAsSb 2.4 μm photodiode detectors,” J. Appl. Phys. **103**, 104511-1-9 (2008).
22. H. Shao, A. Torfi, W. Li, D. Moscicka, and W. I. Wang, “High detectivity AlGaAsSb/InGaAsSb photodetectors grown by molecular beam epitaxy with cutoff wavelength up to 2.6 μm,” J. Cryst. Growth **311**, 1893-1896 (2009).
23. J. W. Zeller, H. Efstathiadis, G. Bhowmik, P. Haldar, N. K. Dhar, J. Lewis, P. Wijewarnasuriya, Y. R. Puri, and A. K. Sood, “Development of Ge PIN Photodetectors on 300 mm Si wafers for Near-infrared Sensing,” Int. J. Eng. Res. Tech. **8**, 23-33 (2015).
24. P. S. Dutta, H. L. Bhat, and Vikram Kumar, “The physics and technology of gallium antimonide: An emerging optoelectronic material,” J. App. Phys **81**, 5821-5870 (1997).
25. A. K. Amerov, J. Chen, and M. A. Arnold, “Molar Absorptivities of Glucose and Other Biological Molecules in Aqueous Solutions over the First Overtone and Combination Regions of the Near-Infrared Spectrum,” J. Appl. Spectrosc. **58**, 1195-1204 (2004).